ELSEVIER

International Journal of Solids and Structures 41 (2004) 801–826

INTERNATIONAL JOURNAL OF SOLIDS and STRUCTURES

www.elsevier.com/locate/ijsolstr

Fully automatic modelling of cohesive discrete crack propagation in concrete beams using local arc-length methods

Zhenjun Yang [a,*], Jianfei Chen [b]

[a] *School of Mechanical and Manufacturing Engineering, Queen's University Belfast, Ashby Building, Strainmillis Road, Belfast BT9 5AH, UK*

[b] *Institute for Infrastructure and Environment, School of Engineering and Electronics, Edinburgh University, The King's Buildings, Edinburgh EH9 3JN, UK*

Received 23 May 2003; received in revised form 11 August 2003

Abstract

A finite element model for fully automatic simulation of multi-crack propagation in concrete beams is presented. Nonlinear interface elements are used to model discrete cracks with concrete tensile behaviour represented by the cohesive crack model. An energy-based crack propagation criterion is used in combination with a simple remeshing procedure to accommodate crack propagation. Various local arc-length methods are employed to solve the material-nonlinear system equations characterised by strong snap-back. Three concrete beams, including a single-notched three-point bending beam (mode-I fracture), a single-notched four-point shear beam (mixed-mode fracture) and a double-notched four-point shear beam (mixed-mode fracture), are modelled. Comparisons of the numerical results with experimental data show that this model is capable of fully automatically modelling concrete tensile fracture process with accurate pre/post-peak load–displacement responses and crack trajectories. Its mesh-objective nature, together with the high efficiency of the energy crack propagation criterion, makes using coarse meshes to obtain reasonably accurate simulations possible. The local arc-length numerical algorithms are found to be capable of tracking complex equilibrium paths including strong snap-back with high robustness, generality and efficiency.

Keywords: Finite element analysis; Discrete crack model; Arc-length method; Mixed-mode crack propagation; Concrete beams

1. Introduction

Developing finite element models (FEM) to simulate tensile fracture behaviour of concrete beams has been extensively carried out in the last two decades. Two types of crack models, i.e., the smeared crack model and discrete crack model, are most frequently used to represent cracking. The smeared crack model

* Corresponding author. Tel.: +44-28-90335523; fax: +44-28-90661729.
E-mail address: z.yang@qub.ac.uk (Z. Yang).

0020-7683/$ - see front matter © 2003 Elsevier Ltd. All rights reserved.
doi:10.1016/j.ijsolstr.2003.09.033

assumes that an infinite number of parallel cracks of infinitely small opening are distributed over the finite element based on a fixed finite element mesh. The crack propagation is simulated by reducing the material stiffness and strength. The constitutive laws are defined by nonlinear stress–strain relations with strain softening. The discrete crack model is based on displacement discontinuity, which is usually represented by nonlinear interface elements. The constitutive behaviour of such elements is represented by softening traction-crack relative displacement relations, as assumed by the cohesive crack model (CCM), or fictitious crack model termed by Hillerborg et al. (1976). The smeared crack model has been much more popular than the discrete crack model because of its computational convenience (e.g., De Borst, 1986, 1987; Rots and De Borst, 1987; Bazant and Lin, 1988; Rots, 1988, 1991; Yamaguchi and Chen, 1990; Malvar, 1993; Bolander and Hikosaka, 1992; Duan, 1994; Foster et al., 1996; Abdollahi, 1996a,b; Ali, 1996; May and Duan, 1997; Ozbolt and Reinhardt, 2002). The latter has been less investigated (e.g., Ingraffea and Gerstle, 1984; Carpinteri, 1989; Bocca et al., 1990, 1991; Rots, 1991; Gerstle and Xie, 1992; Xie, 1995; Xie and Gerstle, 1995; Cendon et al., 2000; Galvez et al., 2002; Yang and Proverbs, 2004), mainly because of various numerical complexities compounded by the constant change of finite element meshes caused by node separation to accommodate crack propagation. Besides a proper constitutive model for concrete tensile softening behaviour, a successful FEM based on discrete crack model must have additional four key features: a proper crack propagation criterion, an efficient remeshing procedure, an accurate mesh-mapping technique to transfer structural responses of an old FE mesh to a new one, and a robust and efficient numerical solution technique to solve nonlinear equation systems characterised with snap-through or snap-back. It is worth noting that besides the traditional smeared crack models and discrete crack models, another attractive type of models recently developed based on embedded displacement discontinuity (Moes et al., 1999; Wells and Sluys, 2000; Alfaiate et al., 2002; Moes and Belytschko, 2002), do not need remeshing.

A proper crack propagation criterion is needed to determine when and in which direction a crack will propagate. The crack is usually assumed to propagate at the direction of the maximum principal stress of the crack-tip node, which is a basic assumption of the original CCM. This direction criterion has been most used. The CCM also assumes that the crack propagates when the maximum principal stress of the crack-tip node reaches concrete tensile strength. This stress-based assumption has been used by most existing studies (e.g., Carpinteri, 1989; Bocca et al., 1990, 1991). Cendon and his co-workers used a maximum tangential stress criterion (Cendon et al., 2000; Galvez et al., 2002). However, nodal stresses are either interpolated from those of integration points in isoparametric finite elements, or are constants when constant strain elements are used. In both cases, very fine crack-tip meshes are necessary to predict accurate stresses. In order to reduce the required mesh density near the crack tip so as to simplify the remeshing procedure, Xie (1995) developed an energy-based cohesive crack propagation criterion. Because of the fast convergence rate of energy entities in FE analysis, crack propagation can be modelled more accurately even using coarse meshes (Xie, 1995; Xie and Gerstle, 1995).

An efficient remeshing procedure is paramount in discrete crack modelling to accommodate crack propagation. The procedures currently available can generally be classified into two categories. One may be termed "remove-rebuild" algorithm. In this algorithm, a new crack-tip node is determined by extending a specified crack growth increment in the calculated propagation direction. The original mesh within a certain range around the new crack-tip node is then completely removed. A complex procedure is followed to form the new crack and regenerate the mesh within this range where a regular rosette is added. This regenerating procedure may be too complicated to be applied to composite structures such as reinforced concrete beams with dissimilar material interfaces. Representatives of such algorithm are the ones developed by Wawrzynek and Ingraffea (1989) and Bocca et al. (1990, 1991). The other type of algorithms may be termed "insert-separate" algorithms such as one developed by Xie in his program AUTOFRAP (Xie, 1995; Xie and Gerstle, 1995). In this procedure, a new edge from the old crack-tip node is first inserted into the local mesh in the propagation direction. The intersection point of this edge with the original mesh is the new

crack-tip node. The new crack is then formed by separating those nodes along the line through the new and old crack-tip nodes. A rosette can be finally added to refine the tip-node mesh. Because this procedure neither completely removes nor rebuilds the new crack-tip mesh as the "remove-rebuild" procedure does, fewer elements are affected and the procedure is much simpler. After remeshing, the structural state variables from the old mesh need to be transferred/mapped as accurately as possible to the new mesh as their initial values to be used in next loading step so as to ensure numerical convergence. The most widely used mapping methods are inverse isoparametric mapping (e.g., James, 1998) and direct interpolation (e.g., Harbaken and Cescotto, 1990).

A variety of numerical procedures have been used to solve nonlinear equation systems associated with material softening, such as Newton iteration and its extensions (e.g., Abdollahi, 1996a,b), dynamic relaxation (Xie, 1995; Xie and Gerstle, 1995), and various arc-length controlled procedures (e.g., De Borst, 1986; Crisfield, 1986; Rots and De Borst, 1987; Crisfield and Wills, 1988; Rots, 1991; May and Duan, 1997; Hellweg and Crisfield, 1998; Alfano and Crisfield, 2001; Crisfield et al., 1997). These solutions, however, have not necessarily led to ideal predictions. Various problems have been reported when the post-peak part of the load–displacement relation is desired, especially when sharp snap-back phenomenon happens in mixed-mode fracture modelling. The Newton iteration methods with load control fail to converge once the limiting point is reached and the post-peak responses cannot be predicted. Displacement controlled Newton methods can tackle structural problems exhibiting snap-through but fail to model snap-back behaviour. The dynamic relaxation method used in a few analyses (Xie, 1995; Xie and Gerstle, 1995) has been criticized for its slow convergence rate and numerical instability due to uncertainties in selecting various pseudo-parameters (e.g., Underwood, 1983). The arc-length method, initially proposed by Riks (1979) and subsequently adapted by Crisfield (1981) and others, succeeded for the first time in tracing the limiting point and post-peak responses by constraining the iterative path along a normal plane or a cylindrical/sphere controlled by a prescribed arc-length. This method has been widely used. However, it has been often reported that these traditional normal-plane and cylindrical/spherical arc-length methods may still fail to converge at or near the limiting points when they are applied to problems involving softening materials (Crisfield, 1986; De Borst, 1986, 1987; Rots and De Borst, 1987; Crisfield and Wills, 1988; Duan, 1994; Crisfield et al., 1997; May and Duan, 1997; Hellweg and Crisfield, 1998; Alfano and Crisfield, 2001). Even the combination of line searches and acceleration techniques (e.g., quasi-Newton) with arc-length method

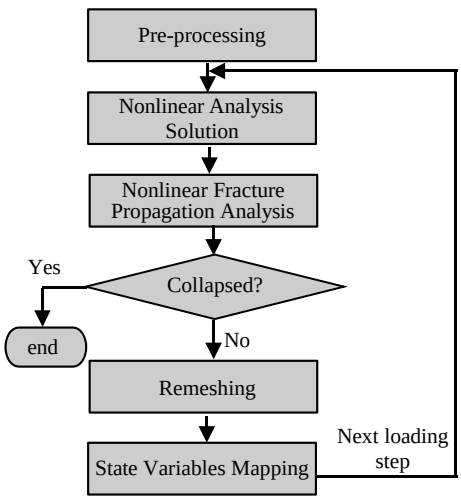

Fig. 1. Key steps of discrete crack FEM.

only achieved limited improvements (May and Duan, 1997). De Borst (1987) and Rots and De Borst (1989) pointed out that this inability should be attributed to the global constrain equations including all the degrees of freedom, which was contradictory to the fact that the failure zone or fracture process zone in concrete beams is highly localised. They thus used only the crack sliding displacement (CSD) and the crack opening displacement (COD) in the constraint equations, respectively. Duan (1994) further devised a new local arc-length procedure to tackle this problem. By automatically distinguishing the strain-localized zones, the selection of relative displacements becomes problem-independent. They reported close agreements with the experimental data based on the local constraint methods using the smeared crack model.

However, very few studies using arc-length methods in the context of discrete crack modelling have been reported. In addition, almost all such studies used pre-defined interface elements. For example, Rots (1991)

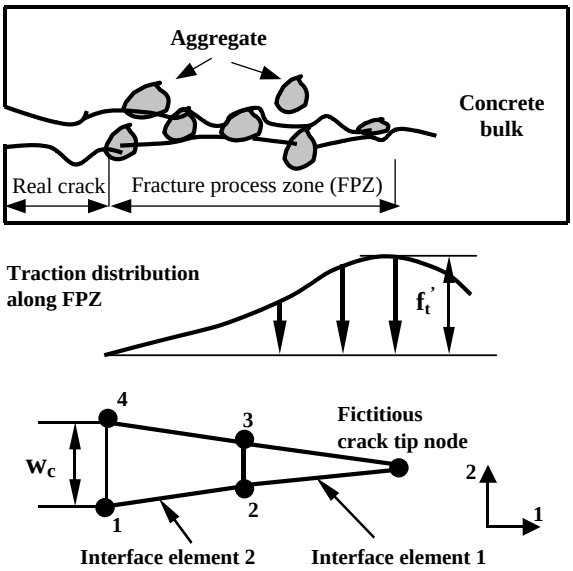

Fig. 2. Modelling of FPZ with four-node interface elements (after Xie, 1995).

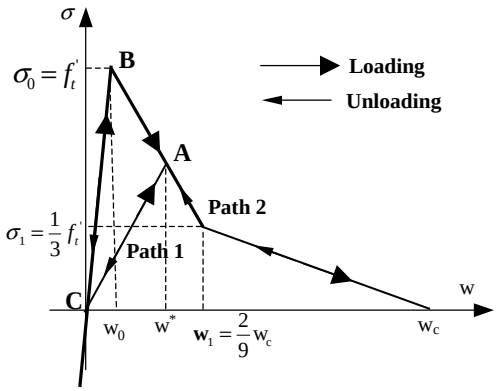

Fig. 3. COD-traction curve of nonlinear interface elements.

used pre-defined interface elements with the COD controlled arc-length method. Alfaiate et al. (1997) developed a "non-prescribed" crack propagation model that limited the cracks along the edges of the finite elements without changing the original FE meshes. This model thus approximates a smooth crack trajectory with a zigzagged one. Recent studies reported by Cendon and his co-workers (Cendon et al., 2000; Galvez et al., 2002) used a two-stage approach: predicting crack paths using linear elastic fracture me-

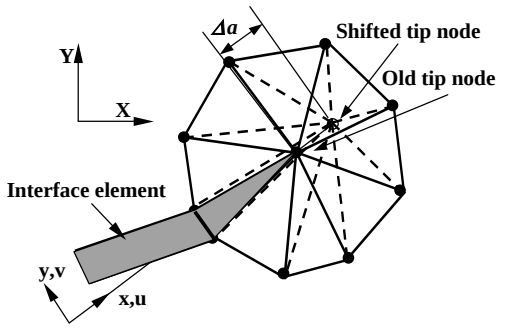

Fig. 4. Coplanar VCE technique for cohesive crack propagation to calculate SERR.

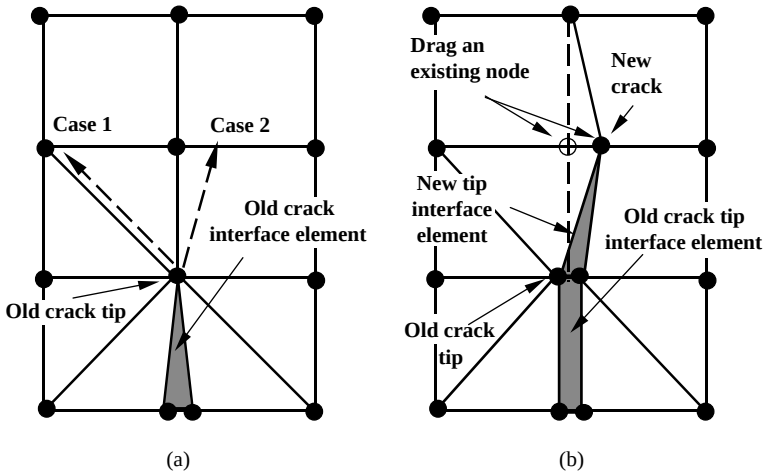

Fig. 5. "Insert-separation" remeshing procedure (after Xie, 1995). (a) Possible crack propagation cases and (b) dealing with Case 2 by dragging a node.

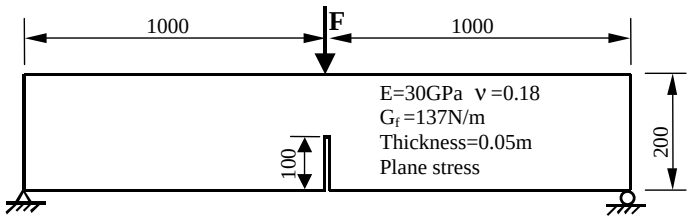

Fig. 6. Three-point bending beam for Mode-I crack propagation (unit: mm).

chanics (LEFM) and incorporating CCM into the crack paths by nonlinear springs. The conclusions drawn from a recent comparative study carried out by the authors (Yang and Proverbs, 2004) was also based on pre-defined crack paths although some initial automatic modelling of crack propagation was carried out on a single-edge notched shear beam. More investigation of the application of arc-length methods to fully automatic discrete crack modelling of fracture process in concrete structures is still desired.

This paper presents a fully automatic discrete crack propagation model for fracture analysis of concrete structures. It uses the remeshing procedure and the energy-based crack propagation criterion proposed by Xie (1995) and Xie and Gerstle (1995). An in-house program, incorporating a modified version of Xie's AUTOFRAP and implementing various numerical techniques, was developed and used in this study. The following first describes the key aspects of the model. Four concrete beams, including a single-edge notched three-point bending beam (mode-I fracture), a single-edge notched four-point shear beam (mixed-mode fracture) and a double-edge notched four-point shear beam (mixed-mode fracture), are then modelled.

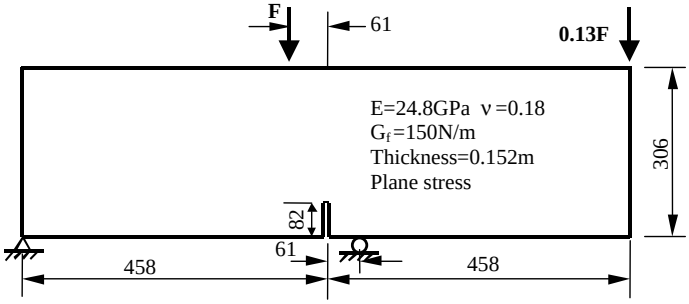

Fig. 7. Four-point single edge-notched shear beam for mixed-mode crack propagation (unit: mm).

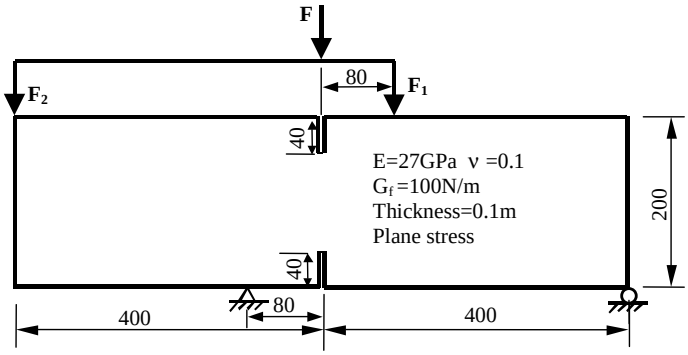

Fig. 8. Four-point DENS for mixed-mode crack propagation with two cracks (unit: mm).

Table 1
Parameters of bilinear COD-traction curves of three example beams

Beam	G_f (N/m)	σ_0 (MPa)	w_0 (mm)	σ_1 (MPa)	w_1 (mm)	w_c (mm)	k_0 (MPa)
SENB	137.0	3.33	0.00001	1.11	0.0329	0.148	33,000
SENS	150.0	4.0	0.00001	1.33	0.03	0.135	40,000
DENS	100.0	2.0	0.00001	0.67	0.04	0.18	20,000

Various local arc-length strategies are examined and their computational efficiency and effectiveness are discussed as well as the robustness and mesh objectivity of the model.

2. Discrete crack finite element model

A thorough description of this model and its computer implementation (Yang, 2002) are beyond the scope of this paper. Fig. 1 illustrates its key steps. The critical physical and numerical aspects of the model are briefly presented as follows.

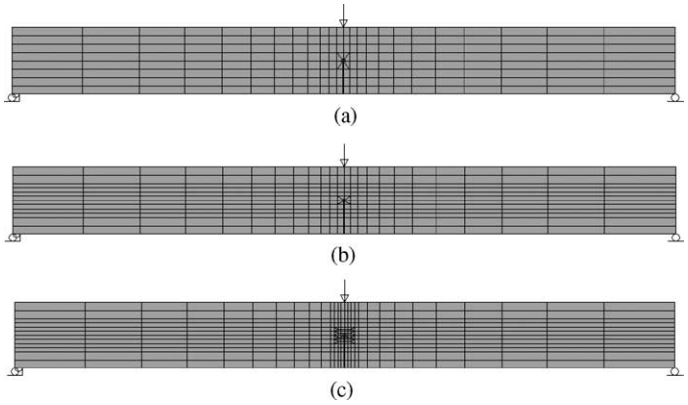

Fig. 9. Initial finite element meshes for SENB beam: (a) $L_{max} > 25$ mm, (b) $L_{max} = 25$ mm and (c) $L_{max} = 10$ mm.

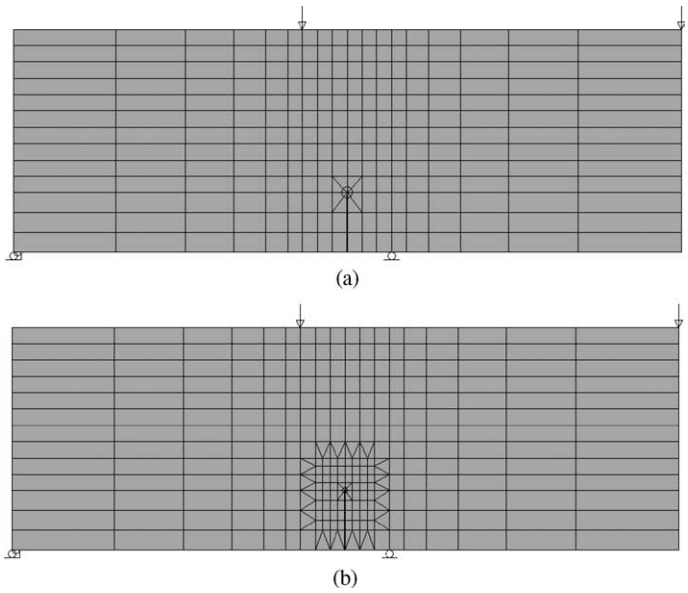

Fig. 10. Initial finite element meshes for SENS beam: (a) $L_{max} > 20$ mm and (b) $L_{max} = 20$ mm.

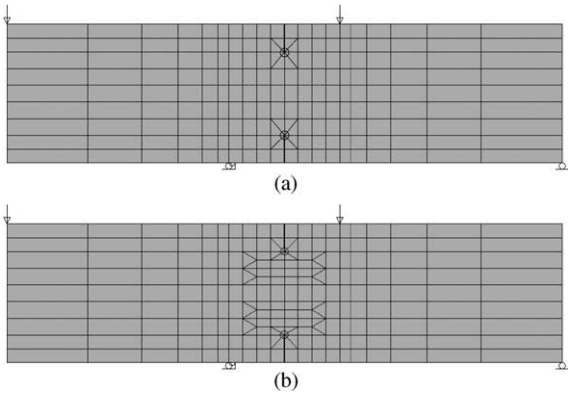

Fig. 11. Initial finite element meshes for DENS beam: (a) $L_{max} > 22$ mm and (b) $L_{max} = 22$ mm.

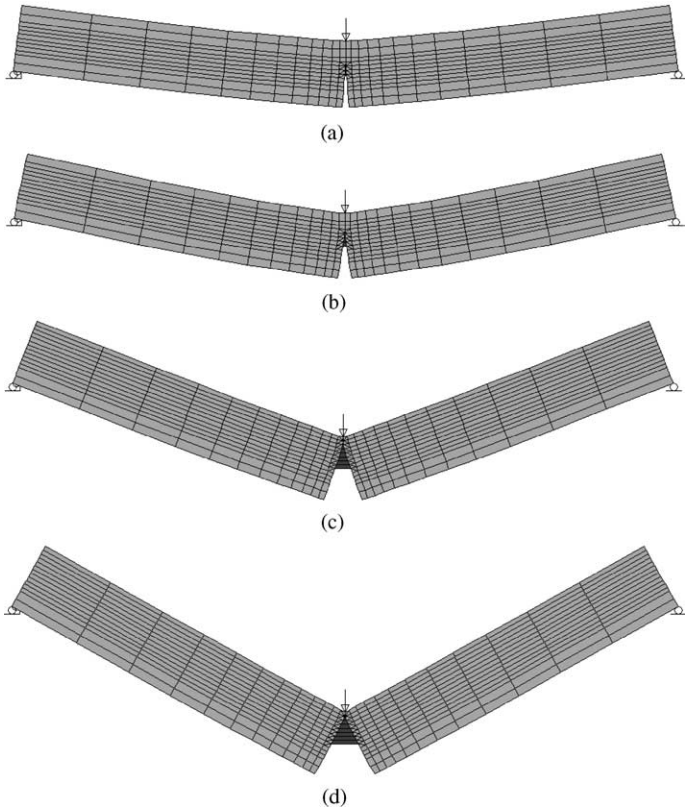

Fig. 12. Cracking process of the SENB beam using $L_{max} = 25$ mm (a) $F = 0.6$ KN, (b) $F = 0.8$ KN (peak load), (c) $F = 0.464$ KN and (d) $F = 0.30$ KN (on collapse): 390 nodes and 9 interface elements.

2.1. Cohesive crack model and unloading paths

CCM can accurately model the energy dissipation process in quasi-brittle materials such as concrete. It assumes that a fictitious crack or a fracture process zone (FPZ) exists ahead of a real crack tip. The FPZ has the capability of transferring stresses through mechanisms such as aggregate interlock and material bonding until the COD reaches a critical value. The CCM has become the basis of nonlinear discrete crack modelling and has been incorporated into some finite element codes in the form of two-dimensional four-node, six-node and three-dimensional eight-node interface elements to model mode-I and mixed-mode crack propagation (e.g., Ingraffea and Gerstle, 1984; Gerstle and Xie, 1992; Xie, 1995; Xie and Gerstle, 1995). The four-node interface elements developed by Gerstle and Xie (1992) are used to represent the cohesive cracks in this study. Fig. 2 schematically shows the FPZ in concrete structures and two interface elements used to model the FPZ.

The Petersson's bi-linear curve (Petersson, 1981) is used here to model the softening behaviour of the cohesive interface elements. Fig. 3 shows the bi-linear COD-traction curve with unloading path indicated. The initial stiffness should be high enough to represent the uncracked material prior to the concrete tensile strength as long as numerical ill-conditioning does not occur. Most existing research used an irreversible unloading path or an elastic damage model (Path 1 in Fig. 3). It assumes that after reaching a value w^*, for decreasing value of w an elastic unloading occurs with a reduced stiffness which represents the secant from the current point to the origin ($A \rightarrow C$) (Rots and De Borst, 1987; Rots, 1988; Rots, 1991; Ali, 1997; Alfaiate et al., 1997; Alfano and Crisfield, 2001). Hellweg and Crisfield (1998) distinguished another unloading mechanism, i.e., reversible unloading, which assumes a completely reversible COD-traction constitutive law (Path 2 in Fig. 3) ($A \rightarrow B \rightarrow C$). Physically, the irreversible unloading represents cracking more realistically than the reversible unloading because when a crack is closing, it cannot transfer higher stresses because the stress-transferring mechanisms such as aggregate interlock and material bonding have been

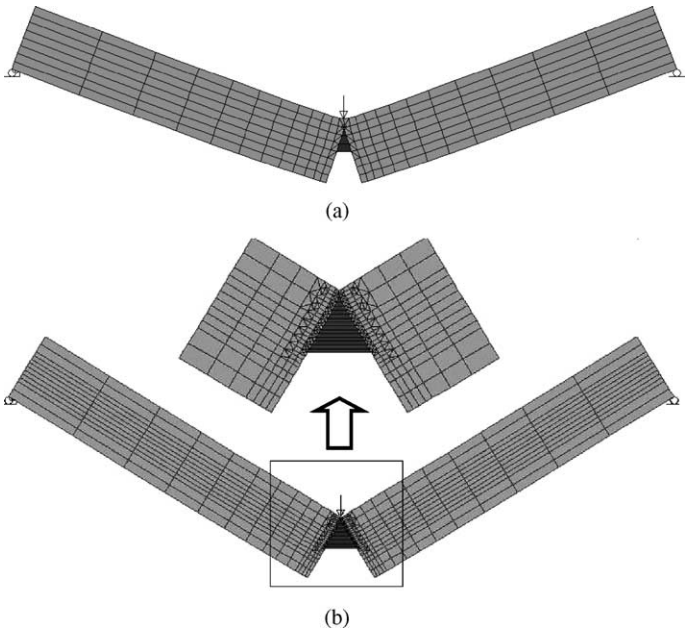

Fig. 13. Deformed configurations of the SENB beam on collapse. (a) $L_{max} > 25$ mm ($F = 0.53$ KN, 242 nodes and 5 interface elements) and (b) $L_{max} = 10$ mm ($F = 0.167$ KN, 513 nodes and 16 interface elements).

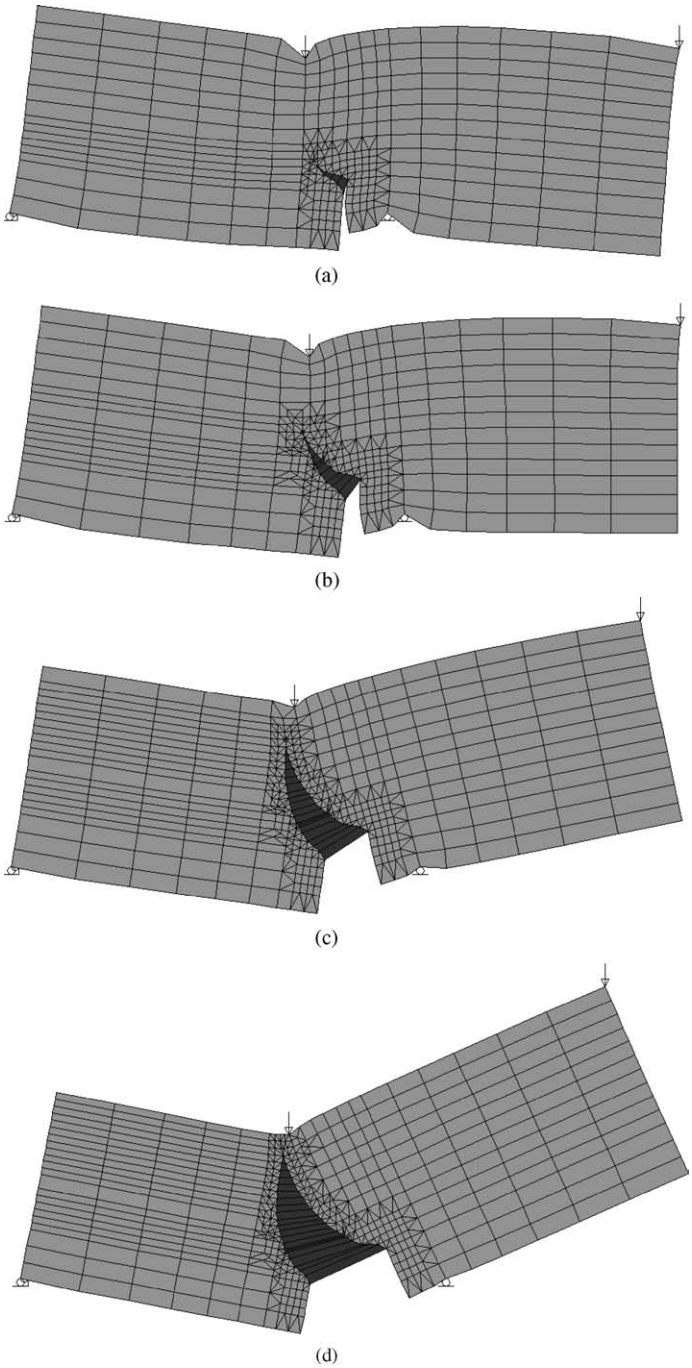

Fig. 14. Cracking process of the SENS beam using $L_{max} = 20$ mm. (a) $F = 140$ KN (peak load), (b) $F = 120$ KN, (c) $F = 60$ KN and (d) $F = 20$ KN (on collapse): 519 nodes and 25 interface elements.

damaged. However, the authors' previous study (Yang and Proverbs, 2004) showed that the unloading paths played an important role in numerical strategies in modelling a mixed-mode concrete beam. In view of this both unloading paths will be investigated in this research.

2.2. Energy-based crack propagation criterion

Based on the principle of energy conservation, Xie (1995) derived the following energy-based cohesive crack propagation criterion

$$G - \mathbf{u}^{\mathrm{T}} \frac{\partial \mathbf{f}}{\partial A} = 0 \tag{1}$$

where $\mathbf{u}$ is the displacement vector, $\mathbf{f}$ is the cohesive forces and A is the crack surface area. G is the total strain energy release rate (SERR) calculated by

$$G = -\frac{1}{2}\mathbf{u}^{\mathrm{T}} \frac{\partial \mathbf{K}}{\partial A}\mathbf{u} + \mathbf{u}^{\mathrm{T}} \frac{\partial \mathbf{P}}{\partial A} \tag{2}$$

where $\mathbf{K}$ is the total stiffness matrix of the elastic bulk and $\mathbf{P}$ the total equivalent nodal force due to external tractions and body forces. In planar mixed-mode fracture problems, the displacement field and SERR can be decomposed to Mode-I and Mode-II components as

$$\mathbf{u} = \mathbf{u}_{\mathrm{I}} + \mathbf{u}_{\mathrm{II}} \tag{3}$$

$$G = G_{\mathrm{I}} + G_{\mathrm{II}} \tag{4}$$

Fig. 4 presents a simple method for conducting a virtual crack extension (VCE) as proposed by Xie (1995) to compute SERR, in which only the crack-tip elements contribute to the energy release rates. By using a finite difference approximation from Eq. (2), the Mode-I and Mode-II SERRs in Eq. (4) may be expressed as

$$G_{\mathrm{I}} = -\frac{1}{2\Delta A}\sum_{i=1}^{N_{\mathrm{ce}}} \mathbf{u}_{\mathrm{I}i}^{e^{\mathrm{T}}} \Delta \mathbf{K}_i^e \mathbf{u}_{\mathrm{I}i}^e + \frac{1}{\Delta A}\sum_{j=1}^{N_{\mathrm{cef}}} \mathbf{u}_{\mathrm{I}j}^{e^{\mathrm{T}}} \Delta \mathbf{P}_j^e \tag{5a}$$

$$G_{\mathrm{II}} = -\frac{1}{2\Delta A}\sum_{i=1}^{N_{\mathrm{ce}}} \mathbf{u}_{\mathrm{II}i}^{e^{\mathrm{T}}} \Delta \mathbf{K}_i^e \mathbf{u}_{\mathrm{II}i}^e + \frac{1}{\Delta A}\sum_{j=1}^{N_{\mathrm{cef}}} \mathbf{u}_{\mathrm{II}j}^{e^{\mathrm{T}}} \Delta \mathbf{P}_j^e \tag{5b}$$

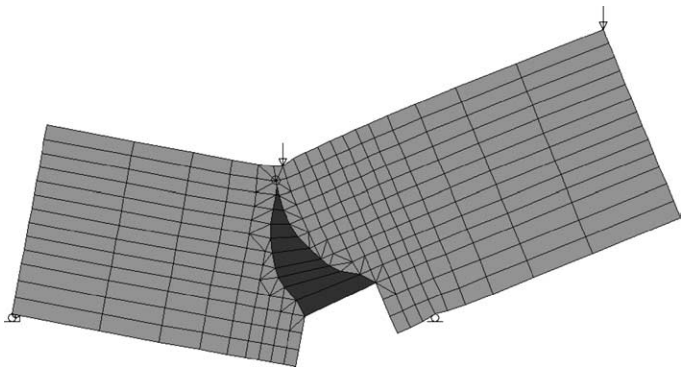

Fig. 15. Deformed configurations of the SENS beam using $L_{\max} > 20$ mm on collapse: $F = 23$ KN, 283 nodes and 11 interface elements.

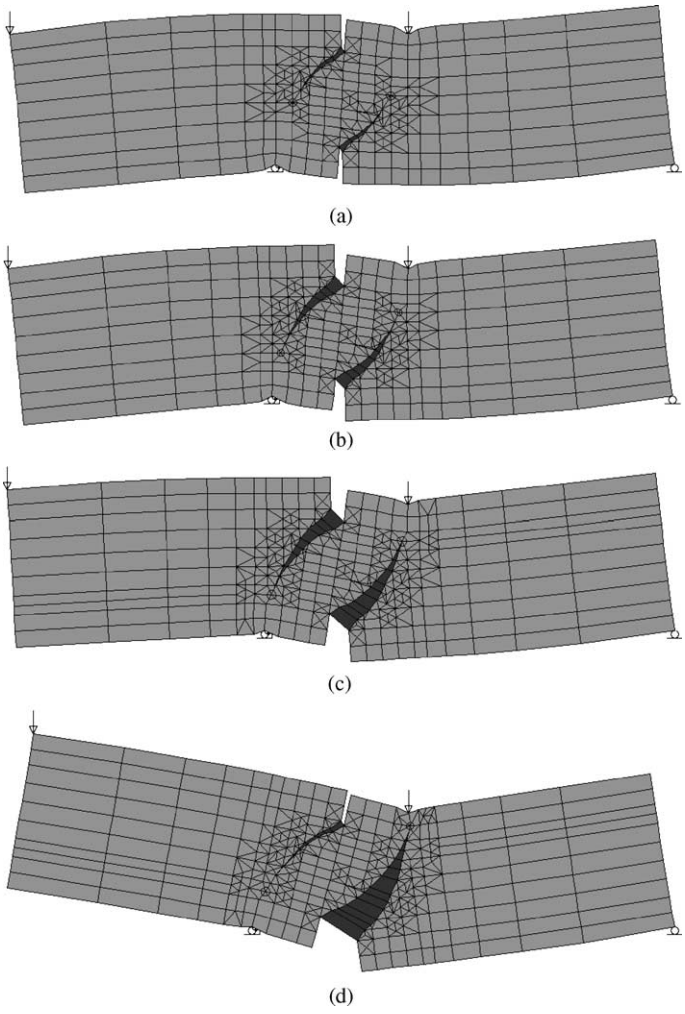

Fig. 16. Cracking process of the DENS beam using $L_{\max} = 22$ mm (a) $F = 42$ KN (peak load), (b) $F = 36$ KN, (c) $F = 27$ KN, (d) $F = 23$ KN: 388 nodes and 24 interface elements.

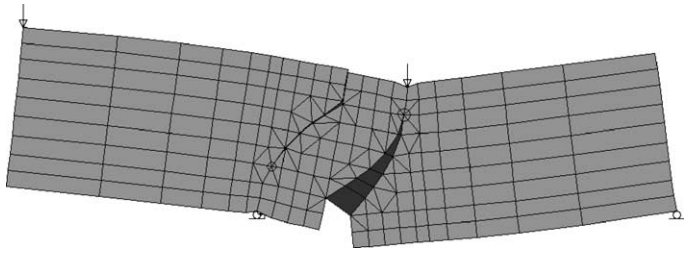

Fig. 17. Deformed configuration of the DENS beam using $L_{\max} > 22$ mm: $F = 20$ KN, 241 nodes, 14 interface elements.

in which N_{ce} and N_{cef} are the total number of elements and the number of elements with applied force around the crack tip respectively; $\mathbf{u}^e_{\mathrm{I}i}$ and $\mathbf{u}^e_{\mathrm{II}i}$ are the Mode-I and Mode-II displacement vectors of the ith

crack-tip element respectively; $\Delta\mathbf{K}_i^e$ is the change of ith crack-tip element stiffness matrix due to VCE; $\Delta\mathbf{p}_j^e$ is the change of the nodal force vector of the jth crack-tip element due to VCE; and ΔA is the increase of crack surface area after a VCE Δa and $\Delta A = t\Delta a$ for a 2D structure with a thickness t.

Interested readers are referred to Yang et al. (2001) for detailed discussion of calculating SERR. The second term of Eq. (1) can be explicitly derived using the four-node interface elements (Xie, 1995). The crack is assumed to propagate in the direction of the maximum principal stress of the crack-tip node.

2.3. Remeshing procedure

When a crack is judged to propagate, a remeshing procedure is carried out to accommodate its propagation. The basic steps of Xie's remeshing procedure (Xie, 1995) are outlined as follows.

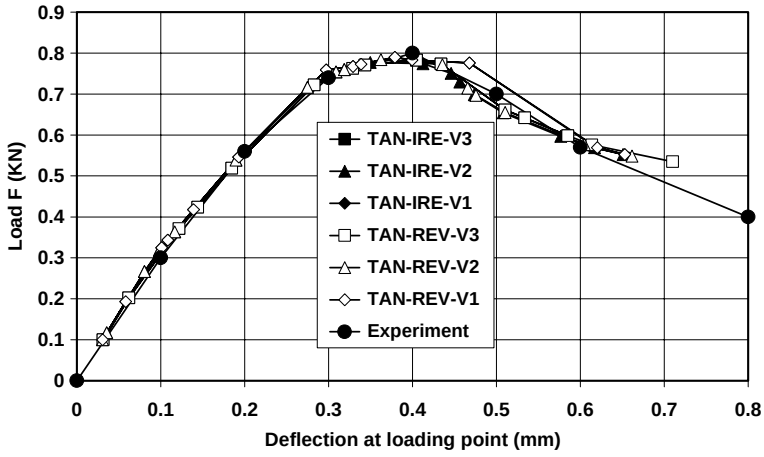

(a)

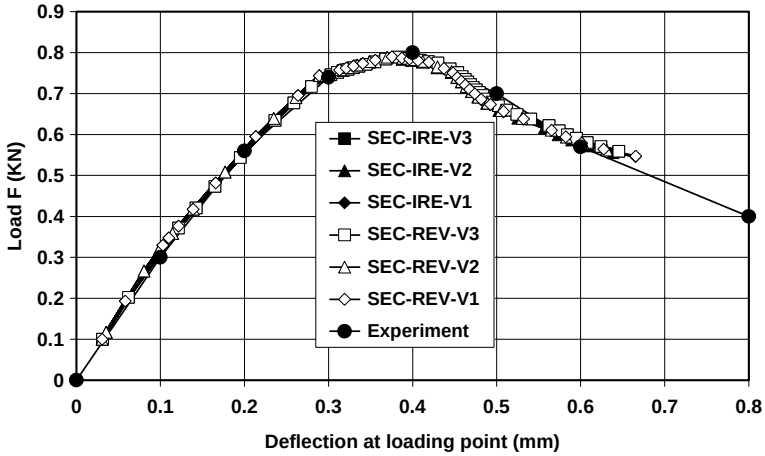

(b)

Fig. 18. Load–deflection curves of beam SENB predicted using mesh Fig. 9a and $N_d = 20$. (a) TAN-based algorithms and (b) SEC-based algorithms.

- delete the existing rosette around the old crack-tip node;
- locate the next tip according to calculated crack propagation direction. Two cases are identifiable (Fig. 5):
  Case 1: the next crack tip is an existing node connected to the old crack tip;
  Case 2: the next crack tip is on the edge of a crack-tip element;
- for Case 1, the edge connecting the new crack-tip node and the old one is split up. For Case 2, the node closest to the new crack-tip position is dragged to the new crack-tip place and is treated as the new crack-tip node. In this way Case 2 becomes Case 1 (Fig. 5);
- refine the new crack-tip mesh according to a specified maximum crack propagation length;
- triangularize all elements around the new crack tip; and
- add a rosette around new crack tip.

For each crack during this procedure, the old three-node crack-tip interface element is altered to a four-node interface element. One three-node tip interface element and one four-node one are created.

2.4. Mesh mapping

The model adopts a direct mapping method proposed by Harbaken and Cescotto (1990). It evaluates the nodal values in the new mesh by directly interpolating those from the old mesh. The following equation is used to map a variable Z, which can be stress, displacement and other state variables at point j

$$Z_j = \frac{\left(\sum_{k=1}^{N} \frac{Z_k}{R_{kj}^2}\right) + \frac{CZ_p}{R_{pj}^2}}{\left(\sum_{k=1}^{N} \frac{1}{R_{kj}^2}\right) + \frac{C}{R_{pj}^2}} \tag{6}$$

where N is the number of points for interpolation in the old mesh, Z_k is the value of Z at the point k, Z_p is the value of Z at the nearest point p to point j, and R_{kj} is the distance between points k and j. The technique requires the user to specify N points for interpolation, the maximum distance $R_{\max}$, the minimum distance $R_{\min}$ and the coefficient C. Those points outside the radius $R_{\max}$ are not considered. If there is a point k very

Table 2
Total number of increments and total iterations for SENB beam

Algorithm	$N_d = 20$		$N_d = 30$	
	Total number of increments	Total number of iterations	Total number of increments	Total number of iterations
SEC-REV-V1	37	814	24	769
SEC-REV-V2	33	668	22	664
SEC-REV-V3	48	1172	25	991
SEC-IRE-V1	37	814	24	769
SEC-IRE-V2	34	681	22	666
SEC-IRE-V3	48	1172	25	991
TAN-REV-V1	15	794	15	597
TAN-REV-V2	17	445	15	610
TAN-REV-V3	16	751	10	1200
TAN-IRE-V1	15	795	13	592 (failed)
TAN-IRE-V2	19	421	15	618
TAN-IRE-V3	14	746	8	580 (failed)

close to j so that their distance is smaller than $R_{\min}$, Z_k is assigned to the value of Z_j. The main advantages of this method are the simplicity and flexibility in choosing C, $R_{\max}$ and $R_{\min}$. Their optimum values to achieve best mapping results are mesh and problem dependent. This study uses a set of empirical values as follows: $C = 0.8$, $R_{\min} = 0.1L_e$ and $R_{\max} = 3L_e$ where L_e is the length of the longest edge of the element in the old mesh in which the mapped point is located.

2.5. Local arc-length method

The comparative study carried out by the authors (Yang and Proverbs, 2004) has shown that the local arc-length algorithms are much more superior than the global ones in terms of numerical robustness and efficiency. The term "global" used herein means that the arc-length constraint equations include all the degrees of freedom whereas only selected degrees of freedom of dominant nodes are included in a "local"

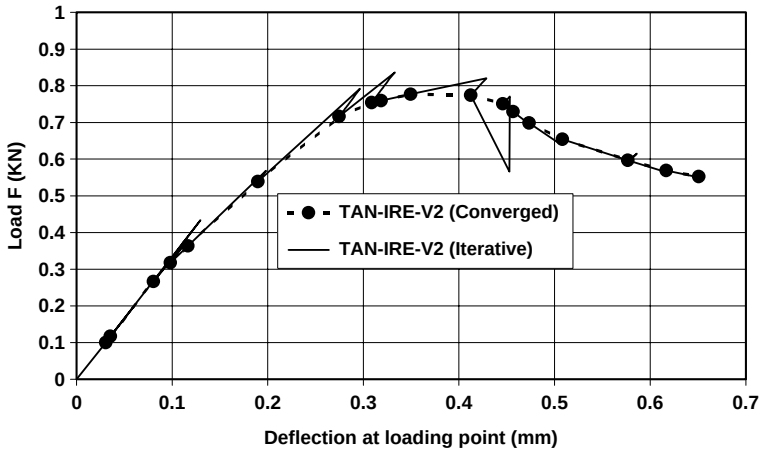

(a)

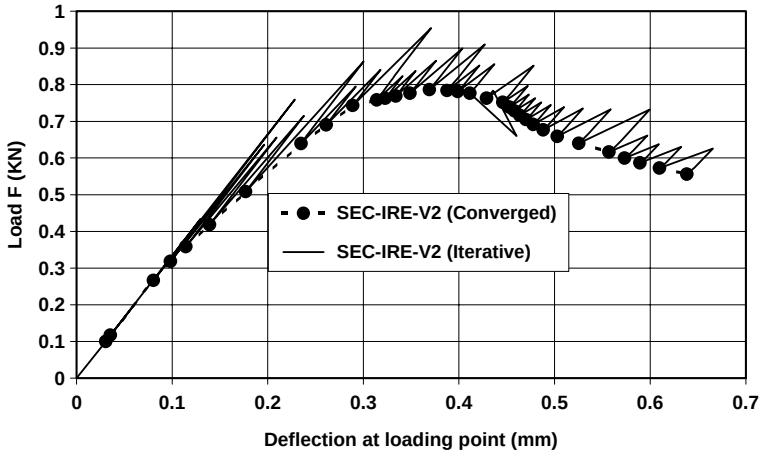

(b)

Fig. 19. Iterative characteristics of TAN/SEC-based algorithms for the SENB beam. (a) TAN-based algorithms and (b) SEC-based algorithms.

arc-length method. The Duan's local updated normal plane constraint equation (Duan, 1994; May and Duan, 1997) is used in this study. The local arc-length formulations in one loading increment can be written as

$$\sum_{\mathrm{e}} \nabla(\Delta \mathbf{u}^{1\mathrm{T}}) \cdot \nabla(\Delta \mathbf{u}^{k}) = l^2, \quad (k = 2, 3, 4, \ldots) \tag{7a}$$

$$\delta\lambda^1 = \frac{l}{\sqrt{\sum_{\mathrm{e}} \nabla(\delta \bar{\mathbf{u}}^{\mathrm{T}}) \cdot \nabla(\delta \bar{\mathbf{u}})}} \tag{7b}$$

$$\delta\lambda^k = \delta\lambda^1 - \frac{\sum_{\mathrm{e}} \nabla(\delta \bar{\mathbf{u}}^{\mathrm{T}}) \cdot (\nabla(\Delta \mathbf{u}^{k-1}) + \nabla(\delta \mathbf{u}^{*}))}{\sum_{\mathrm{e}} \nabla(\delta \bar{\mathbf{u}}^{\mathrm{T}}) \cdot \nabla(\delta \bar{\mathbf{u}})}, \quad (k = 2, 3, 4, \ldots) \tag{7c}$$

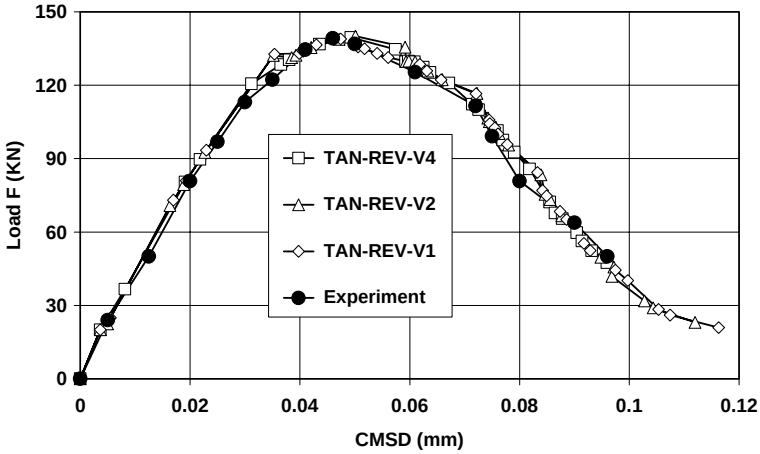

(a)

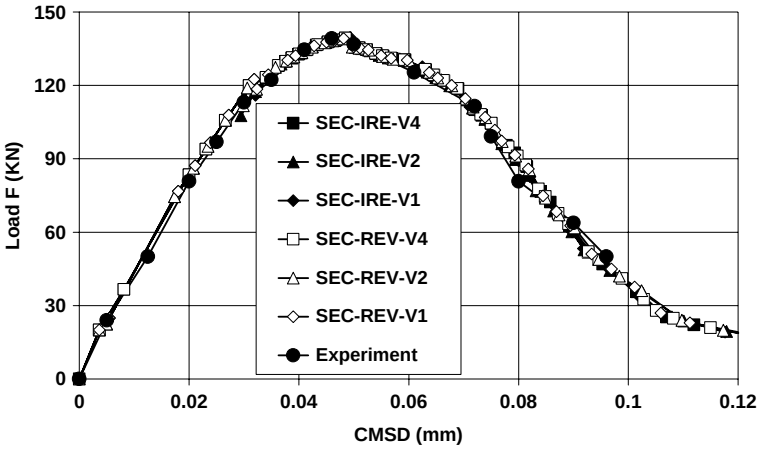

(b)

Fig. 20. Load-CMSD curves of beam SENS: (a) TAN-based algorithms and (b) SEC-based algorithms.

where l is the specified arc-length, $\mathbf{u}$ is the displacement vector and λ is the loading factor. The symbols Δ and δ represent incremental and iterative change respectively. k is the iterative number. $\delta\bar{\mathbf{u}}$ and $\delta\mathbf{u}^*$ are iterative displacement vectors (Crisfield, 1997). Eq. (7a) defines the constraint equations; Eq. (7b) determines the loading factor at the beginning of a loading increment $\delta\lambda^1$; and the iterative loading factors are calculated by Eq. (7c).

The summation in Eq. (7) is calculated in an element-by-element way. Only the elements contributing to structural nonlinearity are included in the constraints. In the smeared crack models, they are finite elements in the damage and failure zones. In CCM based discrete crack models, they are nonlinear interface elements. The symbol ∇ denotes the relative displacement vector (RDV) of dominant elements,

$$\nabla(\mathbf{a}) = [\, a_1 - a_n \quad a_2 - a_1 \quad a_3 - a_2 \quad \cdots \quad a_n - a_{n-1} \,]^{\mathrm{T}} \tag{8}$$

where vector $\mathbf{a}$ is any displacement vector in Eq. (7).

For discrete crack modelling in which the nonlinear interface elements are the dominant elements, another formulation of RDV may include only two CODs and two CSDs of the two pairs of nodes of all four-node interface elements (Fig. 2), i.e.,

$$\nabla(\mathbf{a}) = [\, a_2 - a_8 \quad a_4 - a_6 \quad a_1 - a_7 \quad a_3 - a_5 \,]^{\mathrm{T}} \tag{9}$$

Simpler forms may include only COD or CSD at the crack mouth such as

$$\nabla(\mathbf{a}) = [a_2 - a_8]^{\mathrm{T}} \tag{10a}$$

$$\nabla(\mathbf{a}) = [a_1 - a_7]^{\mathrm{T}} \tag{10b}$$

This set of formulations (Eqs. (7–10)) have three advantages (Duan, 1994; May and Duan, 1997): (i) Eq. (7a) limits the iteration trajectory on a spherical surface, which always has an intersection with the equilibrium path; (ii) it does not need to choose a proper root as spherical/cylindrical constraints do since there is only one root of loading factor; and (iii) the sign of the loading factor will be changed automatically if necessary within the iterations if a total secant stiffness is used; (iv) this local algorithm using RDV guarantees a rapid and stable convergence because it is able to catch the structural nonlinearity and remove the adverse effects of the rigid body movement on the accurate representation of nonlinearity. These advantages have also been demonstrated in (Yang, 2002; Yang and Proverbs, 2004).

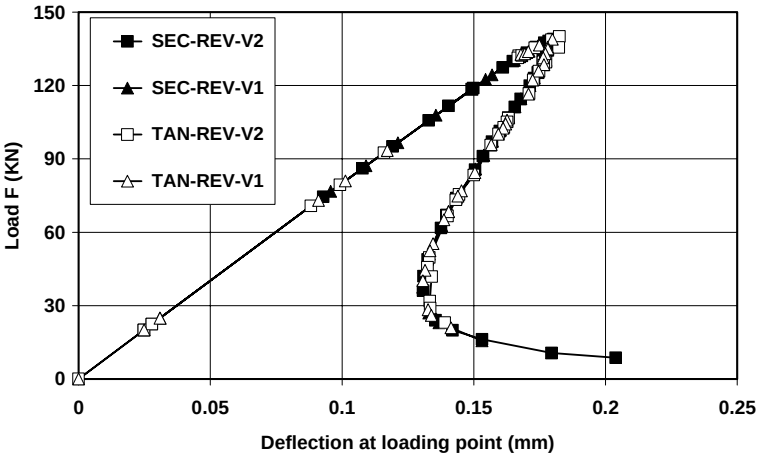

Fig. 21. Load–deflection curves of beam SENS: strong snap-back.

The authors' study has also shown (Yang and Proverbs, 2004) that this constraint method does not inherently defy using the tangential stiffness. When the tangential stiffness is used, Eq. (7b) should be modified as follows

$$\delta\lambda^1 = \mathrm{sign}(|K_t^1|)\frac{l}{\sqrt{\sum_e \nabla(\delta\bar{\mathbf{u}}^T)\cdot\nabla(\delta\bar{\mathbf{u}})}} \tag{11}$$

where $|K_t^1|$ is the determinant of the tangential stiffness matrix K_t^1 calculated at the first iteration of a loading increment.

At the beginning of each loading step, the arc-length l (Eq. (7)) must be determined to ensure the efficiency of the algorithms. Bellini and Chulya (1987) found that the definition of l had a direct effect on the performance of cylindrical/spherical arc-length algorithms applied to geometrically nonlinear problems. The arc-length of the ith loading increment l_i is often predicted by (Crisfield, 1997)

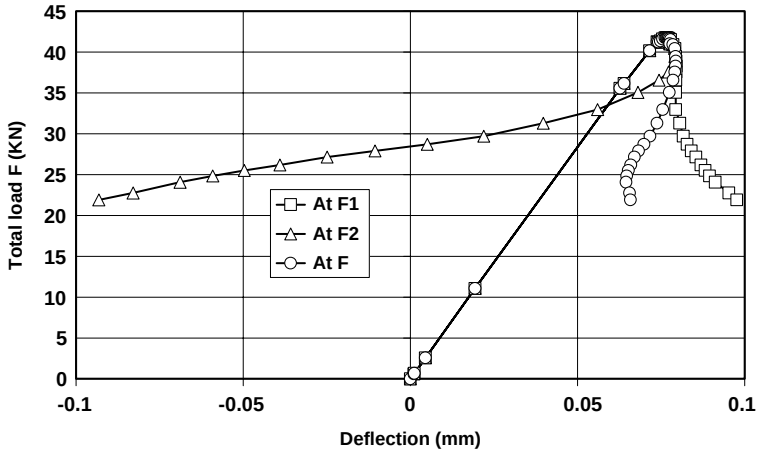

(a)

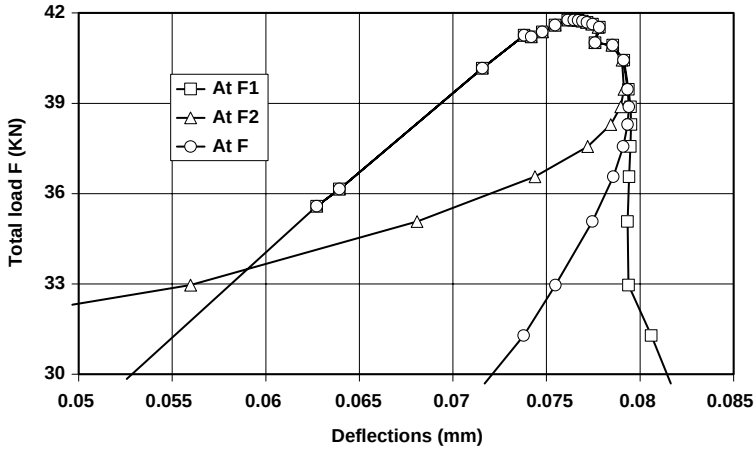

(b)

Fig. 22. Load F–deflection curves of the beam DENS predicted using mesh Fig. 11a and Eq. (14): strong snap-back. (a) Overall and (b) around peak load.

$$l_i = \left(\frac{N_d}{N_{i-1}}\right)^m l_{i-1}, \quad i = 2,3,4,\ldots \tag{12}$$

where N_{i-1} and l_{i-1} are the iteration number and arc-length used by the $(i-1)$th loading step respectively. N_d is a desired optimum iteration number which is problem-dependent. The coefficient m ranges from 0.25 to 0.5 (Bellini and Chulya, 1987). Eq. (12) tends to shorten l to keep the iteration number down when it exceeds N_d.

The arc-length in the first loading increment l_1 can be determined from Eq. (7b) by specifying an initial loading factor based on a proper reference loading condition, e.g., $\delta\lambda^1 = 0.1$. Special considerations are needed for the second loading increment when Eq. (12) is used in some cases. For example, in the three numerical example beams modelled in this study (ref. Sections 3 and 4), there are no initial cracks and thus no interface elements in the first loading increment. Interface elements are added in the second increment. This means all the nodal displacements are used in Eq. (7b) (i.e., global arc-length method), which results in a relatively large l_1. If a comparable l_2 calculated from Eq. (12) is used in Eq. (7b), $\delta\lambda^1$ for the second

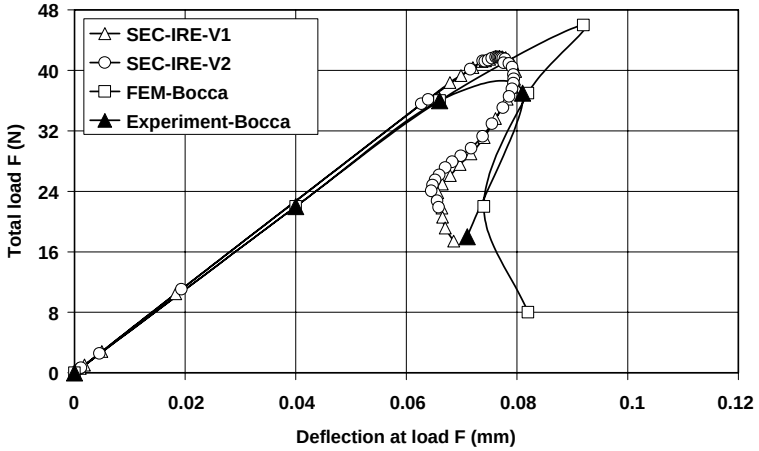

Fig. 23. Load F–deflection curves of the beam DENS predicted using mesh Fig. 11a and Eq. (14): compared with experimental data.

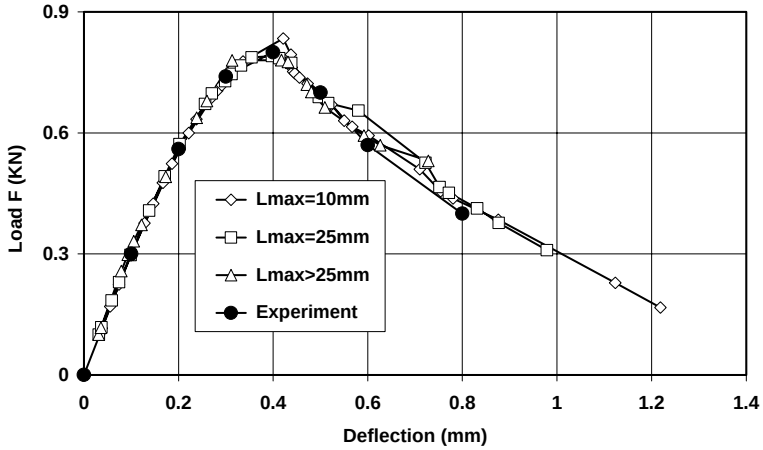

Fig. 24. Load–deflection curves of the beam SENB using different finite element meshes.

loading increment will be very large because only RDVs of the added interface elements are used in Eq. (7b). Too many iterations or even divergence may be caused by the large $\delta\lambda^1$. In order to avoid this, Eq. (12) is modified as

$$\begin{cases} \delta\lambda_i^1 = \lambda_{\text{ini}} & i = 1, \ldots, j \\ l_i = \left(\frac{N_d}{N_{i-1}}\right)^m l_{i-1} & i = j+1, \ldots \end{cases} \tag{13}$$

where j is the loading increment in which the interface elements are first added and λ_{ini} is an initial loading factor for the first j increments. The following default values are used: $N_d = 20$, $m = 0.5$ and $\lambda_{\text{ini}} = 0.1$.

2.6. Iterative numerical algorithms and convergence criterion

The modified Newton–Raphson iterative procedure is used for all the analyses, i.e., the global stiffness matrix is formed at the first iteration of every loading increment and remains unchanged during iterations afterwards.

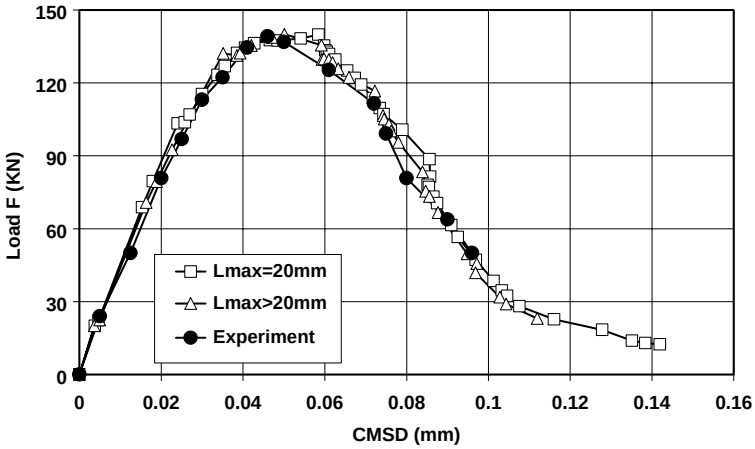

Fig. 25. Load-CMSD curves of the beam SENS using different finite element meshes.

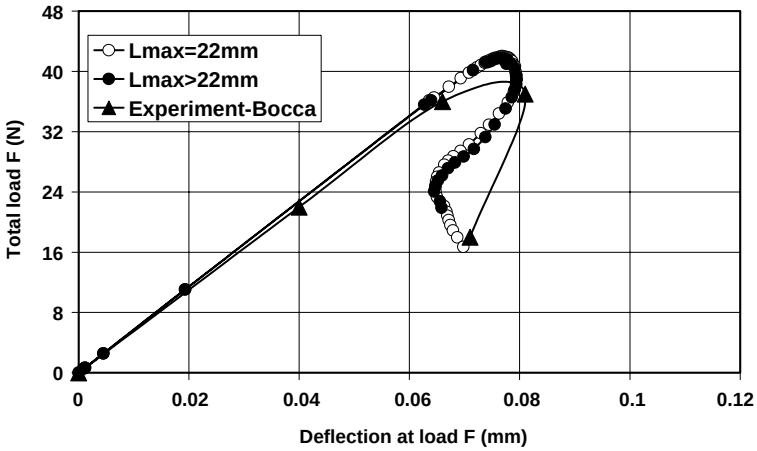

Fig. 26. Load–deflection curves of the beam DENS using different finite element meshes.

The convergence criterion based on the out-of-balance force factor is used for all the analyses, i.e.,

$$\frac{\|\mathbf{r}(\mathbf{u})\|}{\lambda_0\|\mathbf{f}^e\|} \leqslant \beta \tag{14}$$

where $\mathbf{r}$ is the out-of balance force vector, $\mathbf{f}^e$ is the reference loading vector, β is the tolerance, λ_0 is the converged total loading factor of the last loading increment and the norms are Euclidean. A tolerance of 0.001 is used in all the analyses.

The analysis is terminated when any of the following cases is encountered: (i) a crack extends to the finite element boundary; (ii) the iteration number exceeds the specified maximum allowed iteration number (1000 in this study); and (iii) the calculated post-peak load is smaller than a specified one.

3. Numerical examples

Three plain concrete beams with experimental data available are modelled as numerical examples in this study.

3.1. Test setups and material properties

The first example is a single-edge notched beam subjected to three-point bending (SENB). It was tested by Petersson (1981) and modelled by Saleh and Aliabadi (1995) using boundary element method (BEM) and by Xie (1995) using FEM. The geometry, boundary conditions and material properties of the beam are shown in Fig. 6. This is a mode-I crack propagation problem.

The second example is the four-point single-edge notched shear beam (SENS) first tested and analysed by Arrea and Ingraffea (1982). This shear beam has since become a benchmark for the purpose of mixed-mode crack propagation analysis using both FEM (Rots and De Borst, 1987; Xie, 1995; Xie and Gerstle, 1995; Cendon et al., 2000; Yang and Proverbs, 2004) and BEM (Saleh and Aliabadi, 1995). The geometry, boundary conditions and material properties of this beam are shown in Fig. 7.

The third example is the four-point double-edge notched shear beam (DENS) tested and modelled by Bocca et al. (1990, 1991). Two cracks form during the loading process. This may well demonstrate the model's potential to model complex multi-crack propagation. The geometry, boundary conditions and material properties of this beam are shown in Fig. 8.

The shear fracture resistance for the two mixed-mode beams SENS and DENS is simply neglected in this study. This negligence is based on three reasons. Firstly, it has been demonstrated that inclusion of shear traction-CSD curve could only lead to insignificant improvements (e.g., Ali, 1996). Secondly, for these two particular beams, the shear effect is only significant in the initial stage after which mode-I fracture is dominant according to Bocca et al. (1990, 1991). Thirdly, there is a lack of experimental data about the shear traction-CSD curve.

The parameters of the COD-normal traction curves represented by Petersson's bilinear model (Fig. 3) for the three beams are listed in Table 1.

3.2. Finite element modelling

The local arc-length constraint (Eq. (7)) discussed in Section 2.5 can be combined with the other numerical aspects to form various algorithms, which have varying overall numerical effectiveness and efficiency. Among the other factors, the iterative stiffness matrix, the unloading paths (Fig. 3), and the RDVs (Eqs. (8–10)) are the major concerns of this work. For the convenience of discussion thereafter, a numerical algorithm is defined by combining one of the three RDVs, with either the tangent or secant iterative stiffness

matrix, and either the irreversible or reversible unloading path. The following notions are used: TAN for tangential stiffness and SEC for secant stiffness, REV for reversible and IRE for irreversible unloading path, and V1, V2 and V3 for RDVs in Eqs. (8) and (9), and (10) respectively. In this way 12 algorithms are defined. For example, Algorithm TAN-IRE-V1 stands for the local arc-length constraint using RDV of Eq. (8) with the tangential iterative stiffness and irreversible unloading path. The computational effectiveness and efficiency will be examined and compared to each other in the following analysis.

The cracking process of the model is controlled by a maximum crack propagation incremental length $L_{\max}$ which is the maximum allowable crack extension in one loading increment. This requirement is automatically fulfilled by refining crack-tip meshes in the remeshing procedure (Section 2.3). If $L_{\max}$ is specified with a value greater than the greatest initial size of the finite elements around the potential crack path, or with a value greater than the maximum initial size of all the finite elements, no mesh refining operation will occur and the number of loading increments will be closer to the element number in the cracking direction. Otherwise, the crack-tip elements and its surrounding elements will be refined during remeshing to ensure all the actual crack propagation lengths less than $L_{\max}$. More loading steps are therefore modelled, leading to more realistic crack trajectories and smoother load–displacement curves. In this way, only one reasonably fine initial FE mesh is sufficient to achieve required cracking steps determined by $L_{\max}$.

Figs. 9–11 show some initial FE meshes modelled for the three example beams with varying crack propagation control lengths $L_{\max}$. The elastic bulk of concrete is modelled with four-node isoparametric and three-node constant strain elements and cracks are modelled with four-node nonlinear interface elements. The finite element meshes with different mesh density for the same beam will be used for mesh objectivity investigation. A plane stress condition is assumed for all three beams.

4. Results and discussion

4.1. Cracking process and crack trajectory

Figs. 12–17 illustrate some typical successful cracking processes of the three beams, which are fully automatically modelled by the presented discrete crack model. The predicted cracking processes and crack trajectories are in good agreement with the experimental observations. One can see that during the simulation, the finite element meshes are gradually refined around the cracks as they propagate if a smaller $L_{\max}$ is specified. All the displaced configurations use a scale factor of 500.

4.2. Effectiveness and efficiency of the algorithms

All the 12 algorithms are used for the three beams using the initial FE meshes shown in Figs. 9–11.

Fig. 18 shows the predicted load–deflection curves for the beam SENB using the mesh in Fig. 9a and $N_d = 20$. All the 12 algorithms predict the pre/post-peak responses very accurately and effectively up to failure with a load about 0.55 KN.

Table 2 lists the number of loading increments (NOINC) and number of total iterations (NOITE) with two desired iteration number $N_d = 20$ and 30. The following conclusions can be drawn from Table 2: (i) the unloading path has little effect on the effectiveness and efficiency of the algorithms for this beam. This may be due to the monotonic increasing of incremental COD although unloading does happen in some iterations; (ii) the TAN-based algorithms lead to about 35% save of NOITE over the SEC-based ones for RDV2 and RDV3 for $N_d = 20$. The save of NOINC for all three RDVs is more than 100%. This is because the SEC-based algorithms have lower convergence rate and in each loading increment, have averagely more iterations which lead to shorter arc-length l (Eq. (12)) thus more loading increments. The iterative char-

acteristics of TAN/SEC-based algorithms can be clearly observed in Fig. 19. This computational superiority of TAN-based algorithms over the SEC-based ones has also been demonstrated by using pre-defined interface elements (Yang, 2002; Yang and Proverbs, 2004); (iii) a greater $N_d = 30$ reduces the NOINCs of SEC-based algorithms by about 1/3, but NOITEs remain almost unchanged. Using a higher $N_d = 30$ does not make much difference to NOINCs of TAN-based algorithms. It increases NOITEs of TAN-REV-V2, TAN-REV-V3 and TAN-IRE-V2 by 25–35%, and even causes numerical failure to TAN-IRE-V1 and TAN-IRE-V2. Closer examinations showed that the calculation stops from proceeding with the iteration running between two fixed points on an unloading path, which is demonstrated by a constant positive tangential stiffness. This has also been experienced before (Yang, 2002; Yang and Proverbs, 2004); and (iv) the algorithms using RDV (V2) in Eq. (9) saves NOITE by 15–45% over the algorithms using V1 and V3. The reason for this may lie in that Eq. (9) is capable of grasping the nonlinearity more quickly than the other two by including softening-related COD/CSD of all interface elements, whereas Eq. (8) uses RDVs without explicit physical meanings and Eq. (10) uses only one COD/CSD at the crack mouth which is inadequate to fully represent the nonlinearity.

$N_d = 20$ and 30 have also been used to model the beam SENS using the mesh in Fig. 10a and similar four conclusions to the above have been drawn. The specification of N_d is thus very important for numerical efficiency and stability. As cracks propagate, more interface elements are added and thus more RDVs are included in Eq. (7b). Using a constant N_d therefore tends to shorten arc-length l calculated by Eq. (12) and lead to smaller incremental loading factors and thus more increments. Based on extensive simulations, an interface-element-number-dependent N_d is proposed as follows

$$N_d = N_{int}^{\eta} + N_{d0} \tag{14a}$$

where N_{int} is the number of interface elements varying with loading increments and N_{d0} is the initial optimum desired iteration number. $N_{d0} = 10$ is used in this study. The coefficient η is dependent on N_{int} and stiffness matrix. For SEC-based algorithms:

$$\eta = 1.5 \quad \text{when } N_{int} \leqslant 10 \quad \text{and} \quad \eta = 1.2 \quad \text{when } N_{int} > 10 \tag{14b}$$

For TAN-based algorithms:

$$\eta = 1.1 \quad \text{when } N_{int} \leqslant 10 \quad \text{and} \quad \eta = 1.0 \quad \text{when } N_{int} > 10 \tag{14c}$$

The higher η for SEC-based algorithms is used to compensate its slow convergence. Eq. (14) is used for all the following simulations and proves very efficient.

Fig. 20 compares the predicted load-crack mouth CMSD curves for the beam SENS with the experimental data. Again excellent agreements can be seen for both TAN-based and SEC-based algorithms. Fig. 21 presents some predicted load–deflection curves showing strong snap-back behaviour, which is very hard to catch using the other methods.

Numerical difficulties are encountered in modelling the beam DENS with two cracks propagating simultaneously. As for the second beam, all three TAN-IRE-based algorithms fail by oscillation on approaching the peak load. Unexpectedly, the six REV-based algorithms, which work very well for the first two, also fail just before or after peak load is reached. Only the three SEC-IRE-based algorithms successfully trace the full equilibrium paths, one of which is shown in Fig. 22a. The detailed information around the peak load is illustrated in Fig. 22b. It can be seen that initially the three loading points (F1, F2 and F) deflect with the same values. After the peak load, the deflection at Load F2 shows fierce snap-back whereas that at Load F1 continues to increase. This process corresponds to the gradual closure of the upper crack and continuing opening of the lower one (Figs. 16a–d and 17). A real unloading process, at the loading incremental level, therefore takes place. This contrasts with that, in modelling the beams SENB and SENS, only numerical unloading occurs at the iterative level. Therefore, it may be concluded that the REV-based algorithms are unable to model problems with real unloading. This inability may be because they

assume a unloading path that does not represent the real cracking process. It can also be concluded that if real unloading happens, only a SEC-IRE-based algorithm can be reliably used. In this case, relatively high computational cost (although it may still be lower than that from the other methods) should be expected even using a local arc-length method.

Fig. 23 compares the predicted load–deflection relations with the experimental data and FEM results from Bocca et al. (1990, 1991). The deflection at the total load F in Fig. 22 and Fig. 23 is calculated from those at Load F1 and Load F2 assuming that the loading rig using a steel-beam has infinite stiffness. This assumption may cause the discrepancy between the predictions with the experiment data. The discrepancy of current predictions with Bocca et al.'s FEM results may be due to different COD-traction curves used by this study (Petersson's bilinear curve) and them (single linear curve).

4.3. Mesh objectivity

The predicted load–deflection/CMSD curves for the three beams using different finite element meshes whose density is controlled by $L_{\max}$ are presented in Figs. 24–26. For the beam SENB, the numbers of nodes and interface elements of three FE meshes on collapse, i.e., Figs. 13a, 12d, and 13b, are 242 and 5, 390 and 9, and 513 and 16, respectively. For the beam SENS, these numbers of two FE meshes on collapse, i.e., Figs. 15 and 14d, are 283 and 11, and 519 and 25, respectively. They are 241 and 14 (Fig. 17), and 388 and 24 (Fig. 16), respectively for the beam DENS. The huge differences in degrees of freedom, the mesh density and steps of crack propagation make little difference to the predictions in terms of both crack trajectories and load–displacement relations. This well demonstrates the mesh objectivity and robustness of the proposed model and means only a reasonably coarse mesh can lead to accurate simulations. The high numerical efficiency is thus well preserved. The ability of SEC-IRE-based algorithms to model unloading-involved problems with crack closure makes the model a feasible numerical tool to be used in modelling multi-crack propagation under complex loading conditions.

5. Conclusion

This paper has presented a cohesive discrete crack model based FEM for fully automatic simulation of multi-crack propagation in concrete beams. It combines an energy-based crack propagation criterion, a simple remeshing procedure, and various local arc-length numerical algorithms to solve material softening-related nonlinear equation systems. Extensive finite element analyses have been carried out using this model to simulate crack propagation process in three concrete beams under Mode-I and mixed-mode fracture conditions. Comparisons of the numerical results with experimental data show that this model is capable of fully automatically modelling concrete tensile fracture process with accurate pre/post-peak load–displacement responses as well as accurate crack trajectories.

The various local arc-length algorithms are found to be capable of tracking complex equilibrium paths characterised with strong snap-backs due to cracking. In general, the tangential stiffness matrix based algorithms have much higher overall efficiency over the secant stiffness matrix based ones. For problems without real unloading, both reversible and irreversible unloading paths may lead to same predictions. When real unloading takes place, only the irreversible path succeeds in representing the real cracking process. In this case, a secant stiffness matrix must be used to achieve numerical convergence. The RDV, which includes COD and CSD of all interface elements, is found to have highest computational efficiency.

The proposed model is found to have excellent mesh objectivity. This advantage, together with the high efficiency of the energy crack propagation criterion, makes using coarse meshes to obtain reasonably accurate simulations possible. The model may therefore be a feasible numerical tool to be used in modelling multi-crack propagation under complex loading conditions.

Acknowledgements

The authors would like to thank Dr. Ming Xie in Weidlinger Associate INC and Prof. Walter H. Gerstle in the Department of Civil Engineering of New Mexico University in the USA for their kind provision of program AUTOFRAP, a modified version of which has been incorporated into the program developed and used in this research. Their generous contribution is most gratefully acknowledged.

References

Abdollahi, A., 1996a. Investigation of objectivity in the application of the FEM to RC structures-II. Computers and Structures 58 (6), 1183–1211.

Abdollahi, A., 1996b. Numerical strategies in the application of the FEM to RC structures-I. Computers and Structures 58 (6), 1173–1182.

Alfaiate, J., Pires, E.B., Martins, A.C., 1997. A finite element analysis of non-prescribed crack propagation in concrete. Computers and Structures 63 (1), 17–26.

Alfaiate, J., Wells, G.N., Sluys, L.J., 2002. On the use of embedded discontinuity elements with crack path continuity for mode-I and mixed-mode fracture. Engineering Fracture Mechanics 69 (6), 661–686.

Alfano, G., Crisfield, M.A., 2001. Finite element interface model for the delamination analysis of laminated composites: mechanical and computational issues. International Journal for Numerical Methods for Engineering 50, 1701–1736.

Ali, A., 1996. FEM analysis of concrete structures subjected to mode-I and mixed-mode loading conditions. Computers and Structures 61 (6), 1043–1055.

Arrea, M., Ingraffea, A.R., 1982. Mixed-mode crack propagation in mortar and concrete. Report no. 81-13, Department of Structural Engineering, Cornell University.

Bazant, Z.P., Lin, F.B., 1988. Nonlocal smeared crack model for concrete fracture. Journal of Engineering Mechanics, ASCE 114 (11), 2493–2510.

Bellini, P.X., Chulya, A., 1987. An improved automatic incremental algorithm for the efficient solution of nonlinear finite element equations. Computers and Structures 26, 99–110.

Bocca, P., Carpinteri, A., Valente, S., 1990. Size effects in the mixed-mode crack propagation: softening and snap-back analysis. Engineering Fracture Mechanics 35 (9), 159–170.

Bocca, P., Carpinteri, A., Valente, S., 1991. Mixed-mode fracture of concrete. International Journal of Solid and Structures 27 (9), 1139–1153.

Bolander, J., Hikosaka, H., 1992. Applying nonlocal smeared crack concepts to modelling concrete fracture. In: Bazant, Z.P. (Ed.), Fracture Mechanics of Concrete Structures. Elsevier, London, pp. 198–203.

Carpinteri, A., 1989. Size-scale effect on the brittleness of concrete structures: dimensional analysis and snap-back instability. In: Li, V.C., Bazant, Z.P. (Eds.), Fracture Mechanics: Application to Concrete ACI-SP 118. American Concrete Institute, Detroit, pp. 197–235.

Cendon, D.A., Galvez, J.C., Elices, M., Planas, J., 2000. Modelling the fracture of concrete under mixed loading. International Journal of Fracture 103, 293–310.

Crisfield, M.A., 1981. A fast incremental iterative solution procedure that handles ''snap-through''. Computers and Structures 13, 55–62.

Crisfield, M.A., 1986. Snap-through and snap-back response in concrete structures and the dangers of under-integration. International Journal for Numerical Methods in Engineering 22, 751–767.

Crisfield, M.A., 1997. In: Non-linear Finite Element Analysis of Solids and Structures: Advanced Topics, vol. 2. John Wiley and Sons.

Crisfield, M.A., Wills, J., 1988. Solution strategies and softening materials. Computer Methods in Applied Mechanics and Engineering 66, 267–289.

Crisfield, M.A., Jelenic, G., Mi, Y., Zhong, H.G., Fan, Z., 1997. Some aspects of the nonlinear finite element method. Finite Elements in Analysis and Design 27, 19–40.

De Borst, R., 1986. Nonlinear analysis of frictional materials. PhD thesis, Technical University of Delft, Netherlands.

De Borst, R., 1987. Computation of post-bifurcation and post-failure behaviour of strain-softening solid. Computer and Structures 25, 211–224.

Duan, Y., 1994. Non-linear material finite element analysis for concrete and masonry structures. PhD thesis, University of Bradford, UK.

Foster, S.J., Budiono, B., Gilbert, R.I., 1996. Rotating crack finite element model for reinforced concrete structures. Computers and Structures 58 (1), 43–50.

Galvez, J.C., Cervenka, J., Cendon, D.A., Saouma, V., 2002. A discrete crack approach to normal/shear cracking of concrete. Cement and Concrete Research 32, 1567–1585.

Gerstle, W.H., Xie, M., 1992. FEM modelling of fictitious crack propagation in concrete. Journal of Engineering Mechanics, ASCE 118 (2), 416–434.

Harbaken, A.M., Cescotto, S., 1990. An automatic remeshing technique for finite element simulation of forming process. International Journal for Numerical Methods in Engineering 30, 1503–1525.

Hellweg, H.B., Crisfield, M.A., 1998. A new arc-length method for handling sharp snap-backs. Computers and Structures 66 (5), 705–709.

Hillerborg, A., Modeer, M., Petersson, P., 1976. Analysis of crack formation and crack growth in concrete by means of fracture mechanics and finite elements. Cement Concrete Research 6, 773–782.

Ingraffea, A.R., Gerstle, W.H., 1984. Non-linear fracture models for discrete crack modelling. In: Shah, S.P. (Ed.), Applications of Fracture Mechanics to Cementitious Composites, NATO-ARW., September. Martinus-Nijhoff, pp. 247–285.

James, M.A., 1998. A plane stress finite element model for elastic-plastic mode I/II crack growth. PhD thesis, Kansas State University.

Malvar, L.J., 1993. Mixed-mode fracture in concrete. In: Bazant, Z.P. (Ed.), Fracture Mechanics of Concrete Structures. Elsevier, London, pp. 677–688.

May, I.M., Duan, Y., 1997. A local arc-length procedure for strain softening. Computers and Structures 64 (1–4), 297–303.

Moes, N., Belytschko, T., 2002. Extended finite element method for cohesive crack growth. Engineering Fracture Mechanics 69 (7), 813–833.

Moes, N., Dolbow, J., Belytschko, T., 1999. A finite element method for crack growth without remeshing. International Journal for Numerical Methods in Engineering 46 (1), 131–150.

Ozbolt, J., Reinhardt, H.W., 2002. Numerical study of mixed fracture in concrete. International Journal of Fracture 118, 145–161.

Petersson, P.E., 1981. Crack growth and development of fracture zone in plain concrete and similar materials. Report TVBM-1006, Lund Institute of Technology, Lund, Sweden.

Riks, E., 1979. An incremental approach to the solution of snapping and buckling problems. International Journal of Solid and Structures 15, 529–551.

Rots, J., 1988. Computational modelling of concrete fracture. PhD thesis, Technical University of Delft, Netherlands.

Rots, J., 1991. Smeared and discrete representations of localized fracture. International Journal of Fracture 51, 45–59.

Rots, J., De Borst, R., 1987. Analysis of mixed-mode fracture in concrete. Journal of Engineering Mechanics, ASCE 113 (11), 1739–1758.

Rots, J., De Borst, R., 1989. Analysis of concrete fracture in "direct tension". Journal of Solid Structures 25, 1381–1394.

Saleh, A.L., Aliabadi, M.H., 1995. Crack growth analysis in concrete using boundary element method. Engineering Fracture Mechanics 51, 533–545.

Underwood, P., 1983. Dynamic relaxation. In: Belytschko, T., Hughes, T.J.R., (Eds.), Computational Methods in Mechanics for Transient analysis, pp. 245–265.

Wawrzynek, P.A., Ingraffea, A.R., 1989. An interactive approach to local remeshing around a propagation crack. Finite Element in Analysis and Design 5, 87–96.

Wells, G.N., Sluys, L.J., 2000. Three-dimensional embedded discontinuity model for brittle fracture. International Journal of Solids and Structures 38 (5), 897–913.

Xie, M., 1995. Finite element modelling of discrete crack propagation. PhD. thesis, University of New Mexico, USA.

Xie, M., Gerstle, W.H., 1995. Energy-based cohesive crack propagation modelling. Journal of Engineering Mechanics, ASCE 121 (12), 1349–1458.

Yamaguchi, E., Chen, W.F., 1990. Cracking model for finite element analysis of concrete materials. Journal of Engineering Mechanics ASCE 117 (3), 653–673.

Yang, Z.J., 2002. Discrete Crack Modeling of Plated Concrete Beams. PhD thesis, Wolverhampton University, UK.

Yang, Z.J., Proverbs, D., 2004. A comparative study of numerical solutions to nonlinear discrete crack modelling of concrete beams involving sharp snap-back. Engineering Fracture Mechanics 71 (1), 81–105.

Yang, Z.J., Chen, J.F., Holt, G.D., 2001. Efficient calculation of stress intensity factors using virtual crack extension technique. Computers and Structures 79, 2705–2715.